Narrow Line Cooling: Finite Photon Recoil Dynamics

Thomas H. Loftus, Tetsuya Ido, Andrew D. Ludlow, Martin M. Boyd, and Jun Ye

JILA, National Institute of Standards and Technology and University of Colorado, Boulder, Colorado 80309-0440, USA

(Received 12 January 2004; published 13 August 2004)

We present an extensive study of the unique thermal and mechanical dynamics for narrow-line cooling on the $^1S_0$-$^3P_1$ ^{88}Sr transition. For negative detuning, trap dynamics reveal a transition from the semiclassical regime to the photon-recoil-dominated quantum regime, yielding an absolute minima in the equilibrium temperature below the single-photon-recoil limit. For positive detuning, the cloud divides into discrete momentum packets whose alignment mimics lattice points on a face-centered-cubic crystal. This novel behavior arises from velocity selection and "positive feedback" acceleration due to a finite number of photon recoils. Cooling is also achieved with blue-detuned light around a velocity where gravity balances the radiative force.

DOI: 10.1103/PhysRevLett.93.073003 PACS numbers: 32.80.Pj, 32.80.Lg, 39.25.+k, 42.50.Vk

Magneto-optical traps (MOTs) utilizing spin-forbidden transitions have recently attracted considerable attention as starting points for all-optical quantum degenerate gases [1], single-system tests of Doppler and sub-Doppler cooling theory [2], and essential components in the next generation of optical frequency standards [3–5]. Of the currently studied systems, $^1S_0$-$^3P_1$ strontium (Sr) MOTs [6] are particularly relevant to fundamental atomic physics since the single-photon-recoil frequency shift ω_R is comparable to the natural linewidth Γ, and thus ω_R directly influences both mechanical and thermodynamic trap properties. To date, however, many of the rich dynamics for this unique system remain experimentally unexplored.

In this Letter we report a set of novel $^1S_0$-$^3P_1$–driven ^{88}Sr thermal and mechanical dynamics. For laser frequencies (ω_L) tuned below the atomic resonance (ω_A), i.e., $2\pi\delta = \Delta = \omega_L - \omega_A < 0$, trap dynamics separate into three regimes defined by the relative size of $|\Delta|$, Γ, and Γ_E, where $\Gamma/2\pi = 7.5$ kHz and the power-broadened linewidth $\Gamma_E = \Gamma\sqrt{1+s}$ is determined by the saturation parameter $s = I/I_S$. Here I ($I_S = 3\ \mu$W/cm^2) is the single-beam peak intensity ($^1S_0$-$^3P_1$ saturation intensity). Importantly, $\Gamma \sim \omega_R$, where $\omega_R/2\pi = 4.7$ kHz. In regime (I), $|\Delta| \gg \Gamma_E \gg \Gamma$ and semiclassical physics dominates. Photon scattering arises predominantly from single beams over small, well-defined spatial ranges. Gravity also plays an important role as the ratio R of the maximum light-induced acceleration vs gravity $\hbar k\Gamma/2mg$ is only $\sim$16, where $2\pi\hbar$ is Planck's constant, k is the light wave vector, m is the ^{88}Sr mass, and g is the gravitational acceleration. Trapped atoms relocate to vertical positions where magnetic-field-induced level shifts compensate $|\delta|$ and the resultant radiation force balances gravity, leading to δ-independent equilibrium temperatures. In regime (II), $|\Delta| < \Gamma_E, \Gamma_E \gg \Gamma$, a linear restoring force emerges and thermodynamics reminiscent of ordinary Doppler cooling including δ- and s-dependent temperature minima occur, although with values globally smaller than standard Doppler theory predictions. In regime (III), s approaches unity, the photon-recoil-driven impulsive force dominates, and the temperature falls below the photon-recoil limit ($T_R = 2\hbar\omega_R/k_B = 460$ nK, where k_B is Boltzmann's constant) as predicted by a fully quantum treatment [7]. The fact that $\Gamma \sim \omega_R$ also enables observations of novel $\delta > 0$ dynamics, where the ultracold sample divides into momentum packets whose alignment resembles lattice points on 3D face-centered-cubic crystals. This unique behavior, occurring without atomic or excitation coherence, is first explained by an analytic solution to the 1D semiclassical radiative force equation. Here, we show that for $\delta > 0, \Gamma \sim \omega_R$ allows direct visualization of "positive feedback" acceleration that efficiently bunches the atoms into discrete, well-defined momentum packets. The experimentally observed 3D crystal structure is then shown to arise naturally from the 3D excitation geometry. In addition, we experimentally demonstrate that for fixed s, δ determines the lattice point filling factors, results that are confirmed by numerical simulations of the final atomic velocity and spatial distributions. More surprisingly, we find that R directly influences $\delta > 0$ thermodynamics, enabling cooling around a velocity where radiation pressure and gravity balance. The physics underlying this novel behavior is fundamentally the same as regime (I) $\delta < 0$ cooling, but manifest in a dramatically different fashion.

$^1S_0$-$^3P_1$ traps are formed by first precooling ^{88}Sr in a 461 nm $^1S_0$-$^1P_1$ MOT with an axial magnetic-field gradient dB_z/dz (oriented along gravity) of 50 G/cm. The atoms are then transferred to 689 nm $^1S_0$-$^3P_1$ MOTs by rapidly lowering dB_z/dz to 3 G/cm and applying red-detuned broadband frequency-modulated 689 nm light [6]. Over the next 50 ms, the cloud is compressed by linearly increasing dB_z/dz to 10 G/cm. Subsequently, highly stabilized, single-frequency 689 nm light forms the MOT. The optimal transfer efficiency from $^1S_0$-$^1P_1$ MOTs to $^1S_0$-$^3P_1$ MOTs is $\sim$30%, giving final trap populations of $\sim 10^7$. Typical trap lifetimes and spatial densities are $\sim$1 s and $\sim 5 \times 10^{11}$ cm^{-3}, respectively. Trap

dynamics are monitored by either *in situ* or time-of-flight (TOF) fluorescence imaging.

To gain intuitive insight into trap dynamics, we start with the semiclassical expression for the force along z,

$$F(v_z, z) = \frac{\hbar k \Gamma}{2} \times \left[\frac{s}{1 + s' + 4[\Delta - k v_z - g_J \mu (dB_z/dz) z]^2/\Gamma^2} - \frac{s}{1 + s' + 4[\Delta + k v_z + g_J \mu (dB_z/dz) z]^2/\Gamma^2} \right] - mg. \quad (1)$$

where s' ($\geq s$) signifies contributions from other participating beams and $g_J = 1.5$ (μ) is the $^3P_1$ state Lande g factor (Bohr magneton over $\hbar$). The force along x (or y) is similar to Eq. (1), but without gravity. Figure 1(a) presents Eq. (1) for $dB_z/dz = 10$ G/cm, $s = s' = 248$, and a range of δ values. The force is displayed with respect to position (velocity) in the bottom (upper) axis, for v_x or $v_y = 0$ (x or $y = 0$). As δ decreases, the force makes a clear transition from the regime (I) $|\Delta| \gg \Gamma_E \gg \Gamma$ isolated form where excitation occurs over two separate and well-defined spatial ranges to the regime (II) $|\Delta| < \Gamma_E, \Gamma_E \gg \Gamma$ dispersion-shaped form wherein excitation occurs over the entire trap volume and cloud dynamics consist of damped harmonic motion [8]. Correspondingly, as δ decreases, the initially box-shaped trap potential [Fig. 1(b)] becomes progressively more "U"-shaped and the trap shifts vertically upward. Finally, in regime (III) where Γ_E approaches Γ at small s, single-photon recoils dramatically influence trap dynamics which in turn requires a full quantum treatment [7].

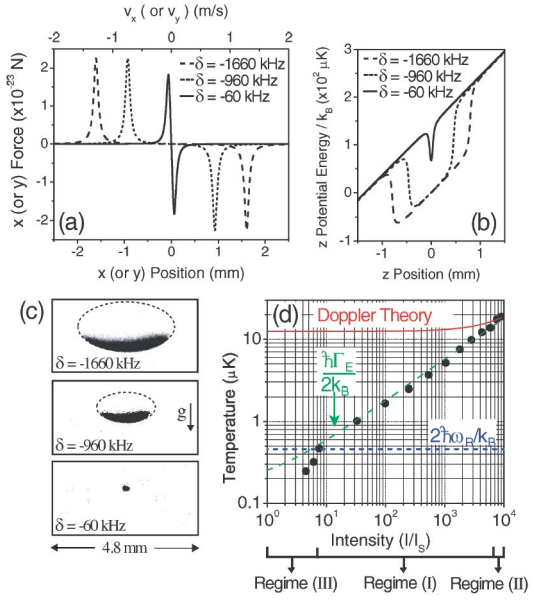

FIG. 1 (color online). (a) Calculated radiative force versus position (bottom axis, $v_x = v_y = 0$) and velocity (upper axis, $x = y = 0$). (b) Trap potential energy in the z direction. (c) *In situ* $^1S_0$-$^3P_1$ trap images. Dashed lines are calculated maximum force contours. For each, $s = 248$ and $dB_z/dz = 10$ G/cm. (d) Temperature vs intensity for $\delta = -520$ kHz and $dB_z/dz = 10$ G/cm. Solid curve: standard Doppler theory; long dashed line: Doppler limit ($\hbar\Gamma_E/2k_B$); short dashed line: single-photon-recoil limit ($2\hbar\omega_R/k_B$); filled dots: experimental data.

Changes in the radiative force are dramatically revealed in trap mechanical dynamics [see Fig. 1(c)]. In the dispersion-shaped cooling regime the cloud aspect ratio is ~2:1, as expected for a typical MOT. Conversely, in the isolated force regime the atoms move freely between "hard wall" boundaries. The cloud horizontal width, therefore, is largely determined by the separation between horizontal force maxima, an effect clearly revealed by the overlaid maximum force contours calculated from Eq. (1). Moreover, since the radiative force is comparable to gravity (recall $R \sim 16$) and the thermal energy is small compared to the gravitational potential energy, atoms sag to the bottom of the trap and the lower cloud boundary z_0 is well defined by the point where the Zeeman shift balances δ.

Studying the MOT temperature versus δ and s also provides rich information about trap dynamics. For large $|\delta|$ and s, corresponding to regime (I), Eq. (1) reflects a balance between gravity and the radiative force from the upward-propagating beam at z_0 [9]. Thus trap thermodynamics are determined by a Taylor expansion of Eq. (1) around $v_z = 0$ for $z = z_0$. With the atomic position (z_0) self-adjusting to follow δ, the damping and momentum diffusion coefficients are δ-independent, giving a predicted equilibrium temperature of

$$T(s) = \hbar\Gamma_E/(2k_B)[0.5R(R - s'/s - 1/s)^{-1/2}]. \quad (2)$$

We have experimentally confirmed this prediction for a wide range of δ [10]. The quantity inside the square brackets is nearly 2, independent of s for the relevant experimental range. Figure 1(d) displays the temperature vs intensity at a fixed large detuning $\delta = -520$ kHz, showing good agreement (aside from a global scaling factor of 2) with the intensity dependence given by Eq. (2). This result arises from the semiclassical nature of regime (I) cooling for which Γ_E is the natural energy scale [11].

For regime (II), $|\Delta| < \Gamma_E, \Gamma_E \gg \Gamma$, Eq. (1) produces a linear restoring force resembling ordinary Doppler cooling. Here, we observe [10] δ- and s-dependent temperature minima with the minimum and its $|\delta|$ location both decreasing with s. Such behavior is predicted by Doppler theory, with the "Doppler limit" achieved at $|\Delta| = \Gamma_E/2$. However, in order to match the data, the theory curves need to be multiplied by a s-dependent global scaling factor (< 1) whose value decreases with s. Moreover, minimum temperatures lie well below the standard Doppler limit of $\hbar\Gamma_E/2k_B$. Notably, this temperature scal-

ing factor is not explained by semiclassical Monte Carlo treatments of the cooling process. In regime (III), $\Gamma \sim \omega_R \sim k_B T/\hbar$ and the radiative force acquires a single-photon-recoil dominated impulsive form. Thus equilibrium thermodynamics can be adequately described only by quantum theory [7]. As shown in Fig. 1(d), the predicted cooling limit of half the recoil temperature $T_R/2 = \hbar\omega_R/k_B$ is experimentally reached as s approaches unity.

Tuning to $\delta > 0$ presents another intriguing set of cooling and motional dynamics. Here, the cloud divides into discrete momentum packets whose alignment mimics lattice points on a three-dimensional face-centered-cubic crystal [12]. Figure 2(a) depicts the underlying momentum-space structure which, as shown below, occurs due to highly directional (i.e., minimal heating) "positive feedback" acceleration and velocity bunching. For the 3D excitation geometry, symmetry dictates that cube corners correspond to three-beam processes while midpoints between corners and cube face centers arise from two- and one-beam processes, respectively. Figure 2(b) shows a δ-specific sequence of top view (slightly off vertical) TOF images for a fixed intensity and atom-light interaction time $t_H = 25$ ms ($t_V = 25$ ms) in the horizontal x-y plane (along z-axis) trapping beams, followed by a free-flight time $t_F = 20$ ms. All images are taken with $dB_z/dz = 0$ although we find qualitatively similar behavior for $dB_z/dz \neq 0$.

At small values of δ (≤ 60 kHz), the atom cloud expands nearly uniformly. As δ increases, three-beam "lattice points" appear first, corresponding to the eight cube corners in Fig. 2(a). This occurs as the cloud is divided into two oppositely moving packets along each of the three axes. When δ reaches a value around 140 kHz, the atom-light interaction becomes sufficiently weak for velocities near zero that some atoms remain stationary along a given axis. These atoms, however, still interact with the beams along the two other axes causing the two-beam lattice points to appear. This process forms a total of 20 divided atom packets with 8, 4, and 8 packets present in the top, middle, and bottom layers of the cube, respectively. As δ increases further, some atoms are left stationary along two axes, enabling formation of the one-beam lattice points, shown as six open circles on the Fig. 2(a) cube face centers. For $\delta > 180$ kHz, the atom-light interaction weakens further and the original atom cloud reappears. We emphasize that the temperature associated with each packet in its moving frame is actually lower than the $t_V = t_H = 0$ atomic cloud. This result arises from the velocity bunching and cooling mechanisms explained below.

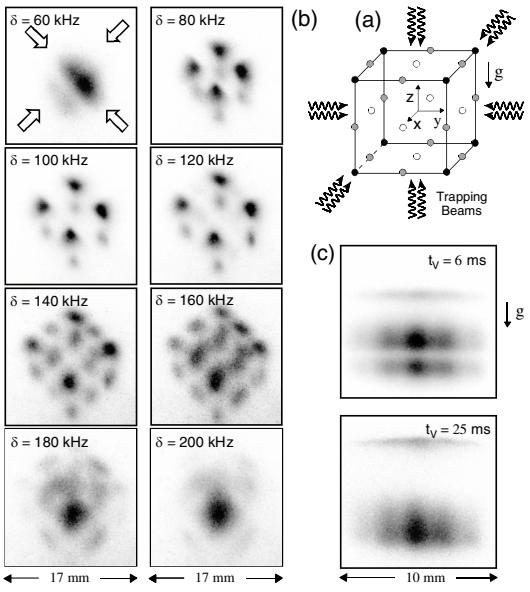

FIG. 2. (a) Underlying momentum-space structure for $\delta > 0$. (b) Top view TOF images for $t_H = t_V = 25$ ms, $t_F = 20$ ms. Arrows in the $\delta = 60$ kHz frame give horizontal trapping beam directions. (c) Side view *in situ* images for $\delta = 140$ kHz and $t_H = 25$ ms. For each, $s = 30$ and $dB_z/dz = 0$.

Only two vertical layers are observed in Fig. 2(b) while Fig. 2(a) predicts the creation of three. This apparent contradiction is resolved in Fig. 2(c), where the cloud is viewed in the x-y plane at 45° to the x, y axes. In order to explore vertical dynamics while maintaining evolution in the horizontal plane, t_H is fixed at 25 ms while t_V is varied between 6 and 25 ms. As before, $t_F = 20$ ms. As shown by the images, the lowest two layers in Fig. 2(a) are only spatially distinct for short t_V, merging together for $t_V = 25$ ms. This occurs as gravity accelerates the middle layer, which is initially stationary along the z axis, into resonance with the downward-propagating laser beam. Subsequently the two downward moving layers merge. Hence, the more (less) intense packets in Fig. 2(b) are due to the lowest two (uppermost) cube layers.

Quantitative insight into $\delta > 0$ dynamics can be obtained from Eq. (1). Recall that for $\delta > 0$, resonant absorption occurs between trapping beams and atoms for which $\vec{k} \cdot \vec{v} > 0$. The absorption process thus preferentially accelerates rather than decelerates the atoms, leading to "positive feedback" in velocity space that terminates at a well-defined velocity set by s and δ. For the unique situation where $\Gamma \sim \omega_R$, system dynamics rapidly evolve toward single-beam interactions. The 1D dynamics can thus be understood by solving Eq. (1) analytically under a single-beam approximation. The full 3D evolution then follows naturally from the 3D excitation geometry. Figure 3(a) illustrates the evolution of the 1D atomic velocity versus interaction time for various s at $\delta = 100$ kHz. Almost independent of the initial velocity (v_i), the mean value and spread of the final atomic velocity (v_f) are set by s and δ, which govern how the acceleration process terminates, leading to efficient velocity bunching. For larger δ or smaller s, a larger fraction of atoms near $v_i = 0$ will remain near $v_f = 0$. Thus a δ- and s-dependent number of velocity bunched groups are

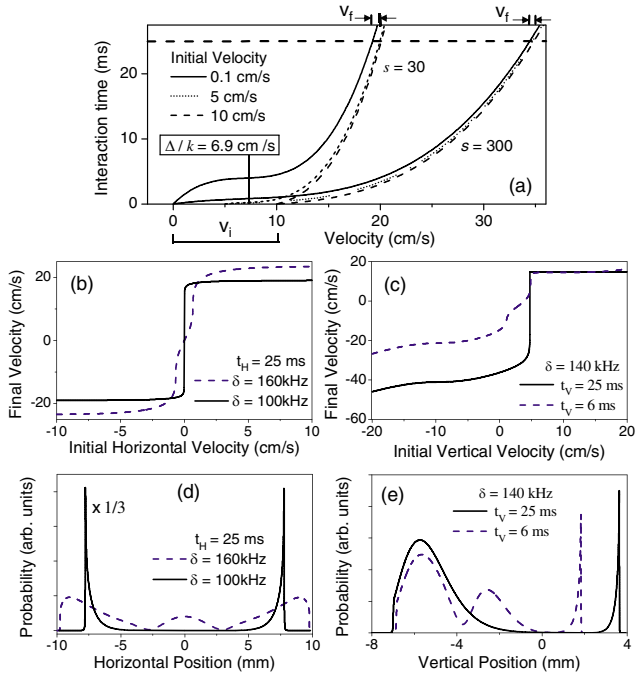

FIG. 3 (color online). (a) Single-beam horizontal acceleration and velocity bunching versus time. Numerically calculated two-beam final versus initial velocity in the (b) horizontal and (c) vertical directions. Corresponding spatial distribution in the (d) horizontal and (e) vertical directions.

formed. Considering horizontal motion first, Fig. 3(b) shows, for $s = 30$ and $t_H = 25$ ms, v_f versus v_i around $v_i = 0$ for $\delta = 100$ and 160 kHz. In the former case, atoms at every v_i are bunched into two groups with $v_f \sim \pm 20$ cm/s. In the latter case, three groups appear at $v_f \sim 0$, 23, and -23 cm/s. Similar dynamics occur in the vertical direction where gravity now plays an important role. Figure 3(c) shows v_f versus v_i for $s = 30$, $\delta = 140$ kHz and t_V times relevant to Fig. 2(c). Notably, for the upward-moving velocity group, even though $\delta > 0$, atoms experience cooling around a velocity v_0 where gravity balances the radiative force, producing the sharp velocity and thus spatial distribution shown in both the experiment [Fig. 2(c)] and theory [Fig. 3(c)]. Theoretically we find the resultant equilibrium temperature is given by Eq. (2), as for the red-detuned case.

For comparison with Fig. 2, Figs. 3(d) and 3(e) give spatial distributions corresponding to the final velocity distributions shown in Fig. 3(b) and 3(c), given the measured initial cloud temperature. Figure 3(d) corresponds to x or y cube axes in Fig. 2(b). Importantly, the model correctly reproduces cloud shape asymmetries [see, for example, the sharp edge on the top of the uppermost layer in Fig. 2(c)], the δ-dependent number of packets and the relative packet populations, and the t_V-dependent number of vertical layers. Predicted final velocities and packet spacings, however, are $\sim$2 times larger than observed. Measuring the position of the upward-moving layer in Fig. 2(c) versus t_V resolves this discrepancy. Measured values for v_f are slightly reduced due to small stray magnetic-field gradients that shift v_0 as the atoms move upward [13], giving an apparent downward acceleration. When these effects are taken into account, predicted and measured positions agree. Finally, we note that $\delta > 0$ momentum-space crystal formation is a universal feature of Doppler limited cooling [10]. For broad line cases where $\Gamma/\omega_R \gg 1$, however, creating structures similar to Fig. 2(b) requires laser beam diameters on the order of tens of centimeters and imaging light with hundreds of megahertz bandwidth, making experimental observations impractical.

In summary, we have performed detailed studies of the transition from semiclassical to full quantum cooling, revealing signatures of each regime without ambiguity. Our results show, for the first time, that the cooling limit of $T_R/2$ can be reached. More surprisingly, when $\delta > 0$, the cold atom sample divides into well-defined momentum packets and cooling is achieved around a velocity where gravity balances the radiative force.

We thank A. Gallagher and J. Hall for useful discussions. This work is funded by ONR, NSF, NASA, and NIST.

[1] Y. Takasu *et al.*, Phys. Rev. Lett. **91**, 040404 (2003).
[2] R. Maruyama *et al.*, Phys. Rev. A **68**, 011403(R) (2003).
[3] M. Takamoto and H. Katori, Phys. Rev. Lett. **91**, 223001 (2003); H. Katori *et al.*, *ibid.* **91**, 173005 (2003); T. Ido and H. Katori, *ibid.* **91**, 053001 (2003).
[4] E. A. Curtis, C.W. Oates, and L. Hollberg, J. Opt. Soc. Am. B **20**, 977 (2003).
[5] G. Wilpers *et al.*, Phys. Rev. Lett. **89**, 230801 (2002); T. Binnewies *et al.*, *ibid.* **87**, 123002 (2001).
[6] H. Katori *et al.*, Phys. Rev. Lett. **82**, 1116 (1999).
[7] Y. Castin, H. Wallis, and J. Dalibard, J. Opt. Soc. Am. B **6**, 2046 (1989); H. Wallis and W. Ertmer, *ibid.* **6**, 2211 (1989).
[8] X.-Y. Xu *et al.*, Phys. Rev. A **66**, 011401(R) (2002); X.-Y. Xu *et al.*, Phys. Rev. Lett. **90**, 193002 (2003).
[9] For the relevant δ range, the atoms do not absorb photons from the downward-propagating beam [see Fig. 1(b)]. Because of polarization considerations, horizontal beam absorption rates are smaller than the vertical rate by 4 times.
[10] A more detailed account of these results will be shown in T. H. Loftus *et al.* (to be published).
[11] P. D. Lett *et al.*, J. Opt. Soc. Am. B **6**, 2084 (1989).
[12] This analogy is not rigorous since face-centered-cubic crystals lack the lattice points along corner connecting lines that are observed in the experiment.
[13] Gravity is not essential to this argument; a similar effect occurs in the horizontal plane.